Surface Microanalysis and Chemical Imaging of Early Dentin Remineralization

Manuel Toledano,[1,*] Inmaculada Cabello,[1] Miguel Angel Cabrerizo Vílchez,[2] Miguel Angel Fernández,[2] and Raquel Osorio[1]

[1]*Faculty of Dentistry, University of Granada, Dental Materials Section, Colegio Máximo de Cartuja s/n, 18071 Granada, Spain*
[2]*Faculty of Sciences, University of Granada, Applied Physics Section, Campus de Fuentenueva s/n, 18071 Granada, Spain*

Abstract: This study reports physical and chemical changes that occur at early dentin remineralization stages. Extracted human third molars were sectioned to obtain dentin discs. After polishing the dentin surfaces, three groups were established: (1) untreated dentin (UD), (2) 37% phosphoric acid application for 15 s (partially demineralized dentin—PDD), and (3) 10% phosphoric acid for 12 h at 25° C (totally demineralized dentin—TDD). Five different remineralizing solutions were used: chlorhexidine (CHX), artificial saliva (AS), phosphate solution (PS), $ZnCl_2$, and ZnO. Wettability (contact angle), ζ potential and Raman spectroscopy analysis were determined on dentin surfaces. Demineralization of dentin resulted in a higher contact angle. Wettability decreased after immersion in all solutions. ζ potential analysis showed dissimilar performance ranging from −6.21 mV (TDD + AS) up to 3.02 mV (PDD + PS). Raman analysis showed an increase in mineral components after immersing the dentin specimens, in terms of crystallinity, mineral content, and concentration. This confirmed the optimal incorporation and deposition of mineral on dentin collagen. Organic content reflected scarce changes, except in TDD that appeared partially denatured. Pyridinium, as an expression of cross-linking, appeared in all spectra except in specimens immersed in PS.

Key words: Raman, contact angle, ζ potential, dentin, demineralization, remineralization

Introduction

Dentin is a dynamic substrate with a complex organic structure. It is a biological composite of a collagen matrix filled with sub-micrometer to nanometer-sized calcium-deficient, carbonate-rich apatite crystallites (≈5 × 30 × 100 nm), dispersed between parallel, micrometer-sized, hypermineralized, collagen-poor, hollow cylinder dentinal tubules containing peritubular dentin (Marshall et al., 1997; Wege et al., 2003).

Accordingly, demineralization of dentin is the process of removing mineral ions from the apatite latticework leaving the collagen fibers without support except for the water contained within the dentin (Bertassoni et al., 2011). Demineralization of dentin, or dentin conditioning, is used as a surface preparation step to improve adhesion for a variety of procedures in restorative dentistry (Toledano et al., 2001). The term remineralization of dentin refers to the process of restoring the inorganic matrix, which is clinically applicable for prevention strategies and therapy of dentin caries and hypersensitivity (Xu et al., 2011; Toledano et al., 2013).

Dynamics involving dentin remineralization are complex. This includes nucleation of minerals, control of post-nucleation growth, and transformation of calcium phosphate deposits to hydroxyapatite (HA) (Hao et al., 2009). Dentin provides both structural and chemical frameworks and is an organic matrix that comprises about 30% type I collagen fibrils and noncollagenous proteins, such as dentin matrix protein and dentin phosphoproteins (Xu et al., 2011). Dentin acts as a scaffold for mineral deposition at specific sites (He & George, 2004). *In situ* specific macromolecules are necessary to function as crystal nucleators, which direct crystal orientation, stabilize the mineral phase, and regulate crystal size (Hao et al., 2009). Thus, nanometer-sized HA develops within a primary template of collagen fibrils to protect them from hydrolytic and enzymatic degradation (Li et al., 2012).

Early stages of dentin remineralization have been scarcely investigated. It has been demonstrated in type I collagen from tendons (Nudelman et al., 2010) that prenucleation clusters are stabilized first, forming loosely packed and diffuse structures of apatite nanocrystals that slowly aggregate and densify. At 10 min, which was the first time period checked, Nudelman et al. (2010) showed the presence of calcium phosphate aggregates 500 nm in size that consisted of densely packed clusters of about 1 nm in size. After 30 min, rapid formation and growth of calcium phosphate particles of 1,000 nm were detected. Concerning particles in solution, Dey et al. (2010) described a subphase consisting of a Tris-buffered solution (pH 7.4) containing only 2.5 mM $CaCl_2$ and 1.0 mM K_2HPO_4 after 1 h, which produced diffraction-amorphous nanoparticles with diameters of 30–80 nm in the bulk solution.

Alternatively, acidic conditioning may damage the structural integrity of collagen. To improve its original integrity, cross-linking, and reinforcement techniques are commonly

*Corresponding author. E-mail: toledano@ugr.es

used (Daood et al., 2013). Biomimetic mineralization imitates the natural process of mineralization, simulating the natural formation process of mineral crystals on the surface of organic and inorganic matrix without using harsh conditions (Xu et al., 2011). Bertassoni et al. (2011) reported some different approaches utilized by other authors, to remineralize dentin. These techniques range from the use of casein phosphopeptide-amorphous calcium phosphate (ACP) proteins or bioactive glass particles to the application of carboxylic acid-containing polyelectrolytes or colloidal nano-beta-tricalcium phosphate. Some other chemical agents may be considered including chlorhexidine (CHX) in solution which produces digluconate anions that may result in gradual precipitation in the presence of other mono- and divalent cations in the substrate (Zerella et al., 2005). Recently, Kim et al. (2011) stated that 1 min of 2% CHX application promoted effective remineralization of demineralized dentin. Zinc, which may be considered as a competitive inhibitor of matrix-metalloproteinases (MMPs) (Osorio et al., 2011*a*), exerts a protective effect through binding at the collagen-sensitive cleavage sites of MMPs, contributing to dentin matrix organization and mineralization (Toledano et al., 2012*b*).

Surface properties of dentin and their influence on the effect of remineralization have been insufficiently investigated (Xu et al., 2011). Removal of apatite crystals from demineralized dentin exposes more of the collagen matrix, decreasing the surface energy (Toledano et al., 2012*a*), without promoting wetting because this procedure leads to a hydrophobic surface. The substrate surface energy may be evaluated, after demineralization and when remineralizing, by contact angle (CA) measurements of a reference liquid on the substrate's surface (Toledano et al., 2001). On the other hand, the electrostatic landscape of collagen fibrils makes the collagen a possible nucleator (Silver & Landis, 2011). Nucleation may be enhanced by the presence of interfaces which allow the aggregation and densification of the liquid-like prenucleation clusters (Veis & Dorvee, 2013). The electrophoretic mobility of a liquid-borne particle is related to the electrostatic potential at the shear boundary, which is the imaginary plane at which ions adhere to the particle; this electrostatic potential, the ζ potential, is important in surface interactions, such as mineralization of teeth (Young et al., 1997). Finally, detailed data about microstructure and chemical analysis are essential to understand changes in dentin. Raman spectroscopy is a nondestructive technique, whose bands allow for semi-quantitative estimation of the organic and inorganic composition of teeth (Pascon et al., 2012) and demineralized or remineralized dentin (Wang & Yao, 2010).

The aim of this study was to investigate the physical and chemical changes occurring at early stages of dentin remineralization, when demineralized dentin specimens were immersed for 30 min in different remineralizing solutions. Two null hypothesis were established: (a) CA and ζ potential measurements did not differ after immersing demineralized dentin samples in some remineralizing solutions and (b) changes were not detectable by using confocal Raman spectroscopy.

Materials and Methods

Specimens Preparation

Forty-five extracted noncarious human third molars were obtained from young patients (20–26 years old) with informed consent from donors, under a protocol approved by the Institution Review Board. The teeth were stored in 0.1% (w/v) thymol solution at 4°C and used within 1 week after extraction. Teeth were sectioned at the cementum–enamel junction to remove the roots, after organic debris/calculus extraction. Mineralized dentin discs (0.75 ± 0.08 mm thick and 6.0 ± 0.01 mm diameter) were obtained from the mid-coronal portion of each tooth using a diamond saw under water cooling. Dentin discs were polished with SiC abrasive papers from 800 to 4,000 grit (Struers LaboPol-4) followed by final polishing steps performed using diamond pastes (Buheler-MetaDi, Buheler Ltd., Lake Bluff, IL, USA) 1 μm down to 0.25 μm.

Specimens were assigned to three groups: (1) no treatment (untreated dentin—UD), (2) partially demineralized with 37% phosphoric acid for 15 s at 25°C (partially demineralized dentin—PDD), and (3) totally demineralized with liquid 10% phosphoric acid for 12 h at 25°C (totally demineralized dentin—TDD), following the method described in Carrilho et al. (2010). PDD and TDD were rinsed in deionized water under constant stirring at 4°C for 72 h. Dentin discs were dried over anhydrous calcium sulphate (8 h). The dry mass of each dentin disc was measured with a microbalance. Specimens were rehydrated in 0.9% NaCl containing 10 U/mL of penicillin G and 300 mg/mL of streptomycin for 24 h (pH 7.0).

PDD and TDD were placed in Eppendorf tubes. Five immersion solutions were utilized: (i) artificial saliva (AS) containing 50 mM Hepes (Applichem, Darmstadt, Germany), 5 mM $CaCl_2$, 0.001 mM $ZnCl_2$, 150 mM NaCl, 100 U/mL of penicillin, and 1,000 μg/mL of streptomycin (pH 7.2); (ii) 40 mM CHX digluconate in AS (pH 7.4); (iii) phosphate solution (PS) containing 50 mM Hepes, 1.5 mM $CaCl_2$, 0.90 mM KH_2PO_4, 2 ppm sodium fluoride, 100 U/mL of penicillin, and 1,000 μg/mL of streptomycin; (iv) 3.33 mg/mL of zinc chloride was added to the AS (pH 7.0) ($ZnCl_2$); (v) 10 wt% ZnO was added to AS (pH 7.0). Specimens were incubated at 37°C for 30 min.

CA Measurements

Three specimens were randomly assigned to 13 equal groups (UD, PDD, PDD + CHX, PDD + AS, PDD + PS, PDD + $ZnCl_2$, PDD + ZnO, TDD, TDD + CHX, TDD + AS, TDD + PS, TDD + $ZnCl_2$, PDD + ZnO). CA measurements were undertaken on UD, PDD, and TDD once the specimens were prepared. The rest of the samples were assessed after immersion in solutions for 30 min, as pointed out above.

The captive bubble method was used to examine dentin wettability. The complete procedure was performed under deionized water. This technique consisted of formation of an air bubble in contact with the dentin surface, which was immersed in MilliQ water at constant temperature

(22°C). A u-shaped steel needle subjected to a micropositioning system was employed, in order to place the bubble against the sample. The bubble volumes were within the range of 10–30 μL. CA values were acquired as described by Montes Ruiz-Cabello et al. (2011). Each CA was the average of ten measurements.

Two-way ANOVA and SNK or Student's *t*-tests were applied. Significance was considered at $p < 0.05$.

ζ Potential Determination

The ζ potential of UD (pH 6.1), PDD (pH 6.1), PDD + CHX (pH 6.0), PDD + AS (pH 6.0), PDD + PS (pH 6.0), PDD + $ZnCl_2$ (pH 6.0), PDD + ZnO, TDD (pH 6.2), TDD + CHX (pH 6.1), TDD + AS (pH 6.2), TDD + PS (pH 6.2), TDD + $ZnCl_2$ (pH 6.1) was measured by dynamic light-scattering, by means of a Zetasizer nano ZS90 (Malvern Instrument, Worcestershire, UK). This equipment measures the electrophoretic mobility of colloid particles in an applied electric field. The laser light illuminates the moving particles, and the velocities of these particles are calculated based on Doppler frequency shifts of the scattered laser light onto four photodiodes fixed at four different angles. The measurements were automatically transformed by autocorrelators to electrophoretic mobility histograms or ζ potential distributions. The Helmholtz–Smoluchowski formula (Chun et al., 2003) was used to determine the ζ potential deduced from the electrophoretic mobility based on the assumption that the double electric layer thickness is small compared with the colloid particle diameter.

Three dentin wafers, one per group, were subsequently pulverized to powder with a steel grinder (Retsch MM400, Biometa, Oviedo, Spain). Dentin powder was then vigorously shaken in a tube agitator (Vortex Wifar, Ref 51075, Velp Scientifica, Milan, Italy), for 5 min. Samples were pipetted from the top 3 mL of the sedimented suspensions from each dentin group, so that only the finest particles would be obtained (Young et al., 1997), and were then measured at 25°C with the Zetasizer nano sample cell system.

Two-way ANOVA and SNK or Student's *t*-tests were applied. Significance was considered at $p < 0.05$.

Confocal Raman Spectroscopy Evaluation

Surfaces (UD, PDD, PDD + CHX, PDD + AS, PDD + PS, PDD + $ZnCl_2$, PDD + ZnO, and TDD) were analyzed with a computer-controlled confocal laser Raman apparatus equipped with a Zeiss optical microscope with a 100× objective and CCD detector attached to a modular research spectrograph (JASCO/NRS-5100; JASCO Europe S.R.L., Milan, Italy). A near-infrared diode laser spot size of <1 μm operated at 785 nm was used to induce the Raman scattering effect. The spectral coverage of this model ranged from 200 to 1,700 cm^{-1}. Calibration of the wavelength and intensity was performed according to manufacturer's specification using a silicon standard and calibration system integrated with the JASCO Spectra Analysis software.

The organic component of dentin was analyzed by examining the following parameters.

Amide III, CH, and amide I: Peaks at 1,246/1,270, 1,450, and 1,667 cm^{-1}, assigned to amide III, CH, and amide I, respectively, are sensitive to the molecular conformation of the polypeptide chains (Xu & Wang, 2011).

Phenyl group: The peak at 1,003 cm^{-1}, which is assigned to the C–C bond in the phenyl group, was used for normalization (Xu & Wang, 2011).

Pyridinium ring vibration: In the spectra, the peak appearing at 1,032.7 $cm^{-1}$was assigned to the C–C in the pyridinium ring vibration that has a trivalent amino acid cross-linking residue (Daood et al., 2013). The relative intensity of this peak increases after the cross-linking formation.

The mineral component of dentin was analyzed examining the following parameters.

The apparent relative mineral concentration of each sample was inferred from the visible ratio of intensities of the peaks at 960 and 1,003 cm^{-1} of HA and the aromatic ring of phenylalanine (phenyl group) residues in collagen, respectively.

Crystallinity was evaluated based on the full-width at half-maximum of the phosphate band at 960 cm^{-1} (Schwartz et al., 2012).

The apparent gradient in mineral content was assessed as the relationship between the ratio of heights at 1,070 cm^{-1} (carbonate) to 960 cm^{-1} (phosphate) and the stretching band of HA.

Two-way ANOVA and SNK or Student's *t*-tests were applied. Significance was considered at $p < 0.05$.

Results

CA Measurements

Mean and standard deviation values for the CA attained in each experimental group are displayed in Table 1. Multiple ANOVA indicated that both dentins ($F = 2{,}553.93$; $p < 0.001$) and solutions ($F = 302.353$; $p < 0.001$) had a statistically significant effect on the observed CA. At baseline conditions, the UD showed the lowest CA. TDD samples attained the highest CA. When PDD samples were immersed in AS wettability was similar to the control PDD. Specimens immersed in CHX and PS attained the lowest CA values within the PDD group showing that PS had the highest wettability. When TDD specimens were immersed in the different solutions, wettability increased (CA decreased) in all groups in comparison with the control TDD group. TDD samples immersed in AS and CHX attained lower CAs than $ZnCl_2$, ZnO, and PS, which performed similarly. In general, PDD specimens immersed in the different solutions were more wettable than the corresponding samples of the TDD group.

ζ Potential Measurements

Mean and standard deviation for the ζ potential values attained in each experimental group are displayed in Table 2. Multiple ANOVA indicated that both degree of mineralization ($F = 580.49$; $p < 0.001$) and solutions ($F = 1{,}103.81$; $p < 0.001$) had a statistically significant effect on the ζ

Table 1. Mean and Standard Deviation of Observed Contact Angle (°) (CA) Measured with Deionized Water on Dentin Surfaces after the Different Experimental Treatments.

30 Min Immersion	Untreated Dentin	PA—Partially Demineralized Dentin	PA—Completely Demineralized Dentin	ANOVA or Student' *t*-Test Results
No immersion	14.89 (1.09) **1**	22.21 (1.44) **2a**	49.84 (2.03) **3a**	$F = 2{,}822.83$; $p < 0.001$
CHX solution		18.88 (1.08) **1c**	25.56 (1.78) **2c**	$t = 185.71$; $p < 0.001$
Artificial saliva		22.43 (1.39) **1a**	25.78 (1.65) **2c**	$t = 43.38$; $p < 0.001$
Phosphate solution		16.91 (1.23) **1d**	29.21 (1.72) **2b**	$t = 610.92$; $p < 0.001$
Cl_2Zn solution		20.68 (1.13) **1b**	30.38 (1.82) **2b**	$t = 368.46$; $p < 0.001$
ZnO solution		19.87 (1.91) **1b**	29.53 (1.99) **2b**	$t = 219.60$; $p < 0.001$
ANOVA results		$F = 44.05$; $p < 0.001$	$F = 403.64$; $p < 0.001$	
Multiple *R*: 0.87				
	Main effects: $F = 756.49$; $p < 0.001$			
	Dentin: $F = 2{,}553.93$; $p < 0.001$			
	Solution: $F = 302.353$; $p < 0.001$			
	Interactions: $F = 281.357$; $p < 0.001$			

Identical letters indicate no significant difference between solutions and numbers between dentin demineralization procedures after Student–Newman–Keuls or Student's *t*-tests ($p < 0.05$). CHX, chlorhexidine; PA, phosphoric acid.

Table 2. Mean and Standard Deviation ζ Potential (mV) of Dentin Powders after the Different Experimental Treatments, Measured in HEPES Buffered Solution.

30 Min Immersion	Untreated Dentin	PA—Partially Demineralized Dentin	PA—Completely Demineralized Dentin	ANOVA or Student's *t*-Test Results
No immersion	−2.18 (0.26) **1**	−2.29 (0.15) **1d**	−0.98 (0.22) **2**d	$F = 33.99$; $p < 0.002$
CHX Solution		1.08 (0.12) **1**b	−0.32 (0.1) **2c**	$t = 1.07$; $p < 0.3588$
Artificial saliva		−1.16 (0.13) **1c**	−6.21 (0.30) **2e**	$t = 932.59$; $p < 0.001$
Phosphate solution		3.02 (0.12) **1a**	0.18 (0.03) **2b**	$t = 2{,}174.02$; $p < 0.001$
CHX solution		1.08 (0.12) **1**b	−0.32 (0.1) **2c**	$t = 1.07$; $p < 0.3588$
Cl_2Zn solution		2.81 (0.31) **1a**	−0.32 (0.05) **1c**	$t = 412.38$; $p < 0.001$
ZnO solution		2.50 (0.26) **1a**	0.06 (0.30) **2bc**	$t = 322$; $p < 0.001$
ANOVA results		$F = 559.45$; $p < 0.001$	$F = 1{,}066.96$; $p < 0.001$	
Multiple *R*: 0.90				
	Main effects: $F = 942.62$; $p < 0.001$			
	Dentin: $F = 580.49$; $p < 0.001$			
	Solution: $F = 1{,}103.81$; $p < 0.001$			
	Interactions: $F = 323.34$; $p < 0.001$			

Identical letters indicate no significant difference between solutions and numbers between dentin demineralization procedures after Student–Newman–Keuls or Student's *t*-tests ($p < 0.05$). CHX, chlorhexidine; PA, phosphoric acid.

potential measurements. At baseline conditions, UD and PDD showed similar ζ potential values, significantly higher than TDD. ζ potential values of dentin specimens within the PDD group showed the following trend: PDD > PDD + AS > PDD + CHX > PDD + PS > PDD + $ZnCl_2$ = PDD + ZnO = PDD+ PS. ζ potential values of dentin specimens within the TDD group showed the following trend: TDD + AS > TDD > TDD + CHX = TDD + $ZnCl_2$ > TDD + ZnO = TDD + PS.

Confocal Raman Spectroscopy

Typical Raman spectra of dentin specimens representing all groups are shown in Figures 1–8.

The peaks at 1,246/1,270 (amide III), 1,450 (CH), and 1,667 (amide I) cm^{-1} became sharper after demineralization (Figs. 2, 3). The shift of bands and the intensity of peaks was recovered after immersion in the different solutions (Figs. 4–8), resulting in stability of the collagen network. Subsequently, amide I and amide III bands manifested a downward shift after immersing the PDD specimens in PS (Fig. 6). The amide III assigned band showed a triple peak within the shift, in AS (Fig. 5), PS (Fig. 6), $ZnCl_2$ (Fig. 7), and ZnO (Fig. 8), whereas the rest of the spectra displayed reflected the standard peaks corresponding to NH and CN bending regions. Signal at 1,003 cm^{-1} (phenylalanine) produced a loss of intensity in CHX (Fig. 4), PS (Fig. 6), and Zn solution (Figs. 7, 8) groups. A slight upward shift in the phenyl peak was observed in PDD (Fig. 2), TDD (Fig. 3), and AS (Fig. 5), where the band came out sharper and accentuated, as evidence of normalization. The pyridinium, as an expression of cross-linking, clearly appeared in all spectra except PS (Fig. 6) that reflected a poor intensity

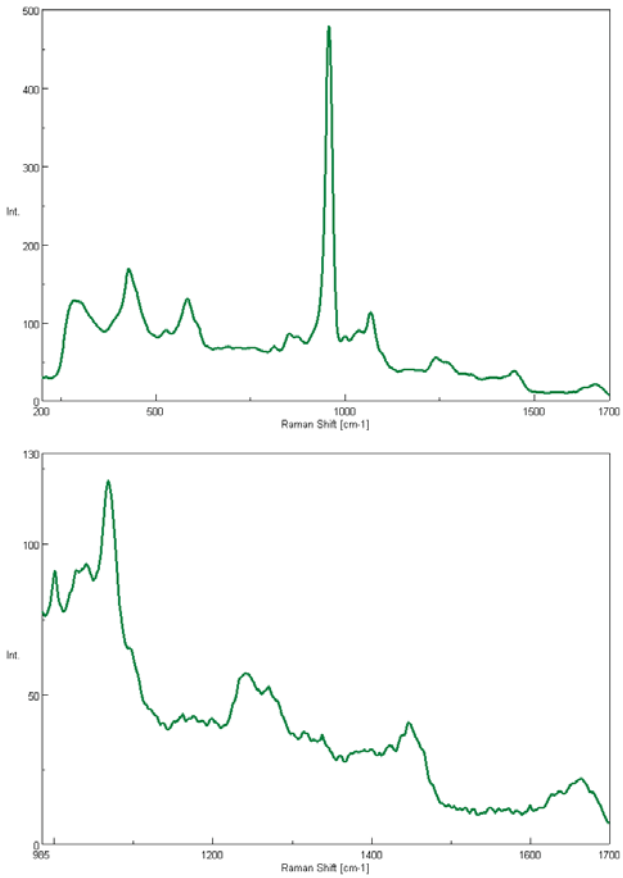

Figure 1. Raman spectra attained from the untreated dentin surface (UD).

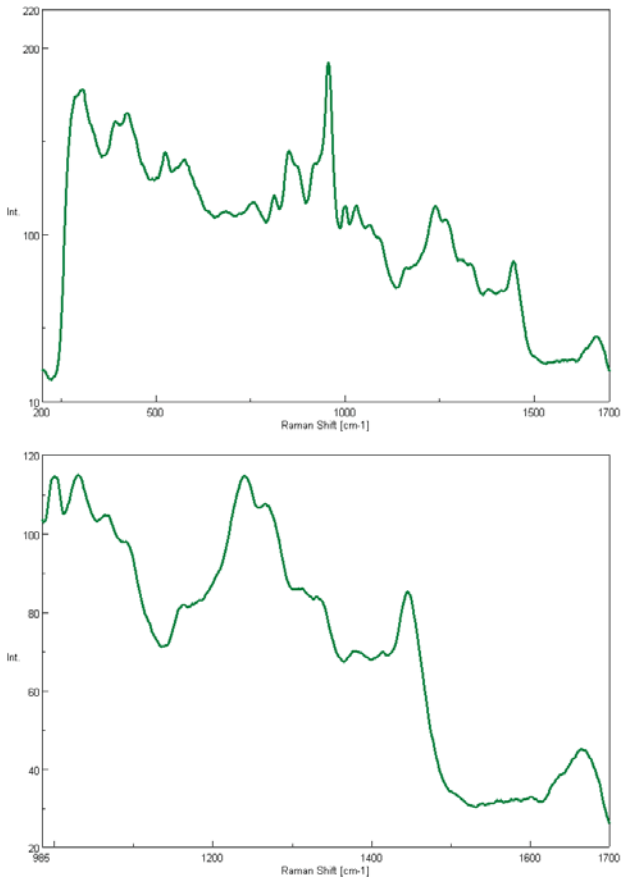

Figure 2. Raman spectra attained from partially demineralized dentin (PDD).

peak at 1,032.7 cm^{-1}. Peaks at 862–869 cm^{-1}, which correspond to hydroxyproline and is associated with the stability of collagen, were remarkable in PDD (Fig. 2), TDD (Fig. 3), and AS (Fig. 5). On the contrary, specimens immersed in PS (Fig. 6) and Zn solutions (Figs. 7, 8) showed the lowest loss of shift intensity. CHX specimens produced a slight upward shift (Fig. 4).

The apparent relative mineral concentration decreased after partial demineralization of dentin, as the 960 cm^{-1} (HA) peak decreased when compared with the peak at 1,003 cm^{-1} (phenylalanine) (Fig. 2). This reduction was much more evident after TDD (Fig. 3). PDD specimens immersed in CHX solution showed (Fig. 4) a pattern of apparent relative mineral concentration quite similar to UD (Fig. 1), but different to the spectra obtained after analyzing the samples immersed in AS (Fig. 5). This analysis demonstrated a well-defined peak of phosphate and carbonate, but the relative intensity of both phenylalanine and hydroxyproline was greater in AS (Fig. 5) than in UD (Fig. 1). Peaks of phenylalanine and hydroxyproline diminished when PDD were kept in PS, demonstrating a larger mineral concentration, as the relative intensity of phosphate and peak of carbonate were high (Fig. 6), which overcame the intensity reported by this mineral in AS (Fig. 5). When dentin specimens were immersed in $ZnCl_2$ and ZnO (Figs. 7, 8), the Raman shift corresponding to the HA band revealed a characteristic relative intensity similar to UD (Fig. 1). An intense loss of crystallinity was observed after demineralization of dentin (Figs. 2, 3). An increase in full-width at half-maximum of the phosphate band at 960 cm^{-1} was detected after immersion of PDD samples in all solutions. Figure 5 describes the crystallinity data in AS. Similar to the crystallinity observations, an overall loss of intensity for the majority of bands involved in the apparent gradient in mineral content is displayed in the spectra measured on demineralized dentin (Figs. 2, 3). A clear phosphate (960 cm^{-1}) and carbonate (1,070 cm^{-1}) stretching led to an increase in the apparent gradient in mineral content in all immersed specimens in remineralizing solutions.

Discussion

Dentin is a mineralized connective tissue. Dentin demineralization can arise from an acid attack by bacteria or the food source, and from acid etching for resin–dentin bonding (Kim et al., 2011). In our study, a pronounced effect on wettability, with CAs increasing dramatically, was determined from the UD to PDD samples and from PDD to TDD (Table 1). Thus, the increased CA and differences between TDD and PDD are believed to be a result of differences in the intrinsic hydrophobicity of the surfaces,

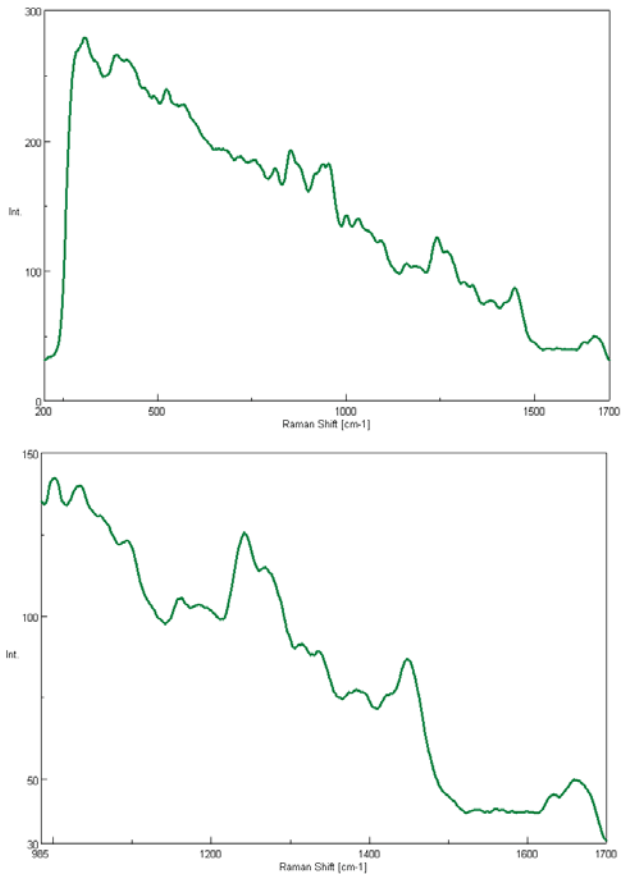

Figure 3. Raman spectra attained from totally demineralized dentin (TDD).

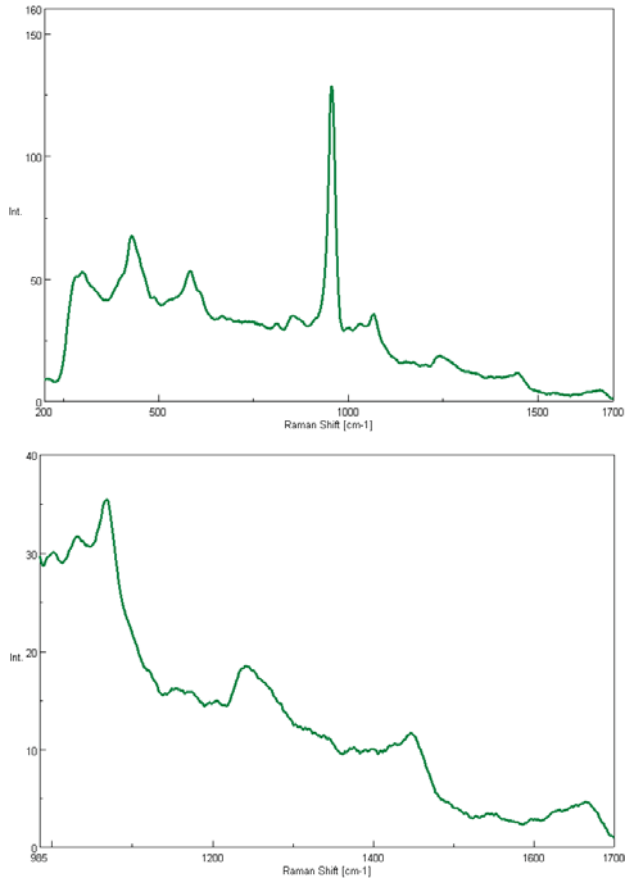

Figure 4. Raman spectra attained from partially demineralized dentin surfaces after 30 min of immersion in chlorhexidine (CHX) digluconate solution (PDD + CHX).

and are therefore suggestive of chemical differences and inorganic content of both kinds of demineralized dentins. Mineral crystallites remaining within the collagen after demineralization (Bertassoni et al., 2010) might have contributed to the decrease in the CA, as there exists a positive correlation between mineral level and spreading capability of a liquid (Panighi & G'Sell, 1992). That is, if the CA is low wettability is high. This demineralizing effect could also be studied after Raman spectroscopy observations. Figures 2 and 3 show a lack of crystallinity and a significant loss of intensity at phosphate (PO_4^{3-}) (960 cm^{-1}) and carbonate (CO_3^{2-}) (1,070 cm^{-1}) peaks, diminishing the apparent gradient in mineral content, which is more pronounced in TDD (Fig. 3) with a lower degree of spectral noise. Similarly, the apparent relative mineral concentration also dropped after the larger recession of the 960 cm^{-1} peak (HA). Furthermore, by comparing the collagen spectra collected from the PDD (Fig. 2) and the UD samples (Fig. 1), it can be observed that the demineralized collagen was not denatured as the spectra were similar. Wang and Yao (2010) indicated that the I and III amide regions in the spectra are known to be very sensitive to the collagen conformation and secondary structure, which shall change if collagen is denatured, as was reflected in the spectra from the TDD samples (Fig. 3), in the bands 1,246/1,270 and 1,667 cm^{-1}.

UD (−2.18 mV) and PDD (−2.29 mV) samples showed similar ζ potential values (Table 2). Similarly, Saito et al. (1998) also obtained equal interfacial tensions between partially dephosphorylated dentin collagen (9.7 mol of P/mol of collagen) and the intact dentin (19.5 mol of P/mol of collagen). The ζ potential and CA results indicate that TDD samples are negatively charged (−0.98 mV), leading to a weakly polar hydrophobic surface (Table 1) resulting in poor remineralization ability (Xu et al., 2011). On the contrary, PDD samples showed a higher negative charge compared with the TDD samples. Xu et al. (2011) proposed that with higher negative charge, the surface of demineralized dentin can attract more calcium ions (positive charge) and thereby enhance the nucleation ability of the surface collagen of PDD; therefore, in TDD sample substrata, the larger electrostatic potential status of particles was achieved, which is directly related to their dispersion stability by electrostatic repulsion. ζ potential can, therefore, be considered as a measure of colloidal stability. The higher the ζ potential values, the higher electrostatic repulsion and therefore colloidal stability (Sadat-Shojai et al., 2010), protecting the particles from aggregation, and resulting in a more stable dispersion of these particles in the dilute solution (Sadat-Shojai et al., 2010; Veis & Dorvee, 2013), in close contact with the dentin substratum.

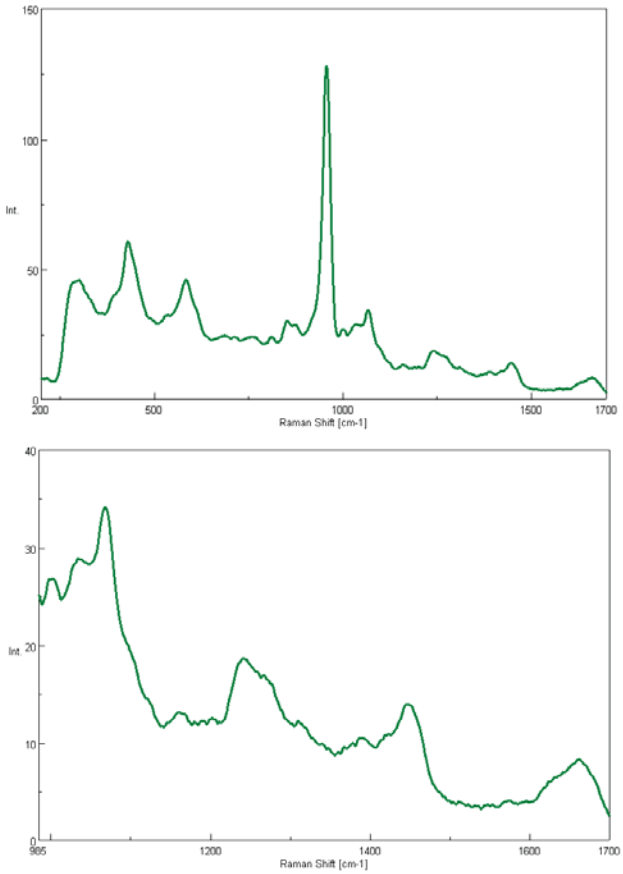

Figure 5. Raman spectra attained from partially demineralized dentin surfaces after 30 min of immersion in artificial saliva (AS) solution (PDD + AS).

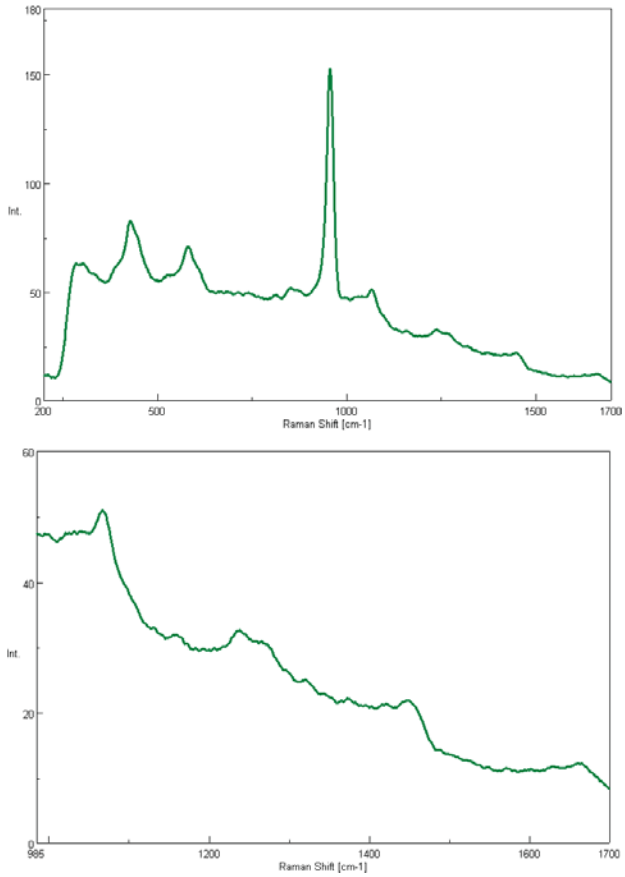

Figure 6. Raman spectra attained from partially demineralized dentin surfaces after 30 min of immersion in phosphate (PS) solution (PDD + PS).

The interfacial free energy is an important factor in regulation of mineralization (Xu et al., 2011). Due to its inherent ability to be retained in dentin matrices (Carrilho et al., 2010), it is generally accepted to apply 2% (~40 mM) CHX to acid-etched dentin during resin-dentin bonds in an attempt to increase the durability of interfaces by inhibiting endogenous MMPs. CHX is a cationic compound that has the ability to bind anionic molecules, such as the phosphate present in the residual HA structure, that remains after partial etching (Wang & Yao, 2010) (Fig. 2) or at the demineralization dentin front. Phosphate exists in the calcium carbonate complex of dentin; therefore, CHX can bind phosphate, which in turn can lead to the release of small amounts of calcium from dentin (Pascon et al., 2012). Moreover, as CHX only binds electrostatically, between the protonated amine groups of CHX and the mineral phosphates to demineralized dentin collagen (Kim et al., 2010), it may slowly diffuse out of a collagen matrix via a competitive desorption mechanism in the presence of other cations. This binding of polyanions and cationic compounds might lead to the deposition of a network of a cluster of ions, molecules and/or particles, stable enough to exist but having neither the size nor the structure sufficient to grow into a crystal on its own, named pre-nucleation clusters. It is important to point out that the initial cluster is presumed to be disordered. The initial prenucleation cluster can be considered as a dense liquid phase, that is, a hydrated aggregate composed of ions, molecules, and/or prenucleation clusters. This has a defined interface that is more dense than the surrounding solution but less dense than the crystal form (Veis & Dorvee, 2013).

Specimens immersed in CHX attained one of the lowest CA values within PDD and TDD groups. Complementarily, wettability of TDD samples immersed in CHX was lower than that obtained in other PDD samples (Table 1). These CA measurements showed that the rate of water entry into the demineralized dentin was enhanced by holding open the intermolecular spaces after partial demineralization of the dentin with higher cross-linking densities (Li et al., 2012) and was larger than in TDD samples.

The Raman results indicate that PDD matrices develop a reduction of cross-links following 15 s of conditioning. It was shown that after immersion for 30 min in all solutions, except in PS (Fig. 6), an increase in the peak intensity at 1,030–1,033 cm^{-1} was observed. This peak is assigned to the C–C in a 3-hydroxypyridinium ring, which is associated with a nonreducible cross-linking formation naturally occurring in collagen (Xu & Wang, 2011). PDD samples immersed in CHX solution showed that the pyridinium ring was present at the same proportional peak intensity with

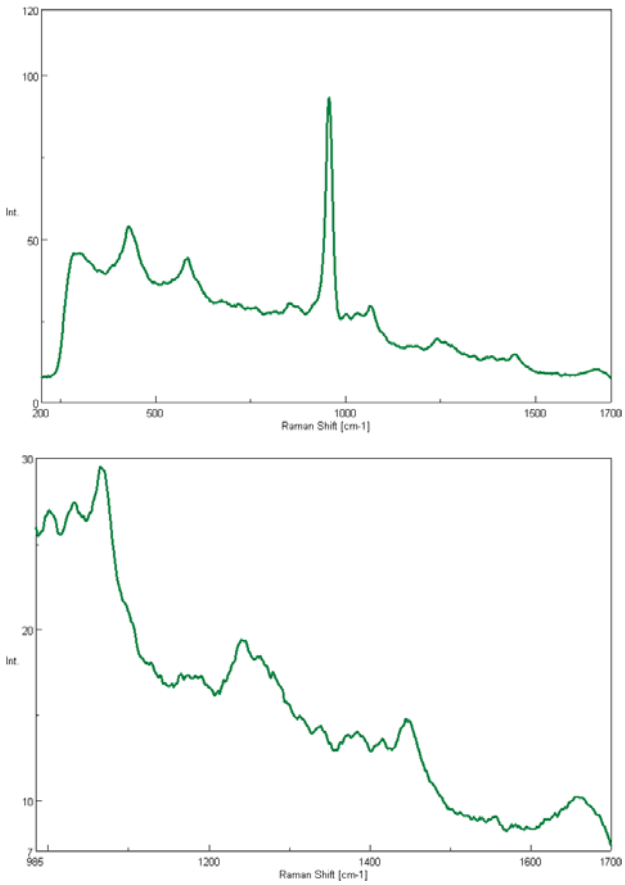

Figure 7. Raman spectra attained from partially demineralized dentin surfaces after 30 min of immersion in $ZnCl_2$ solution (PDD + $ZnCl_2$).

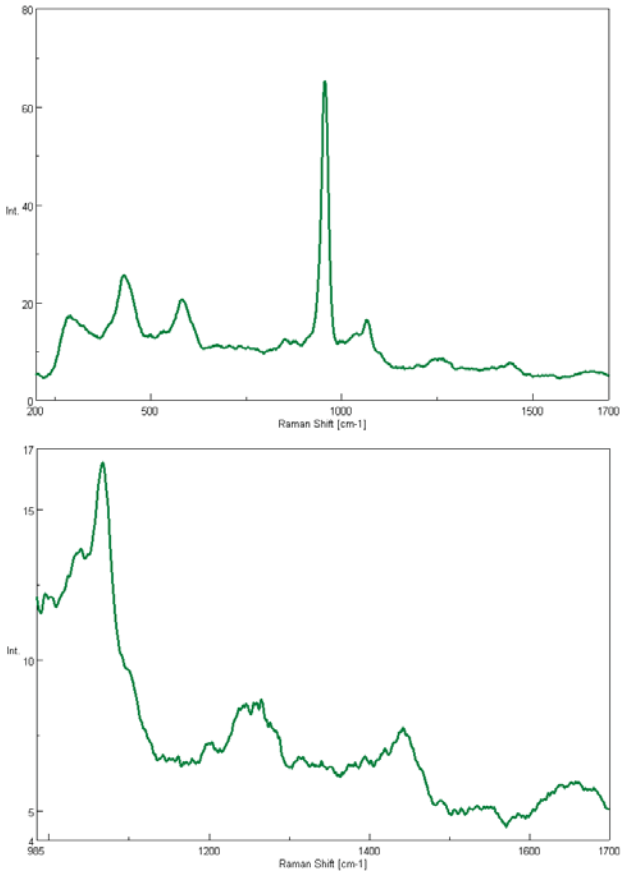

Figure 8. Raman spectra attained from partially demineralized dentin surfaces after 30 min of immersion in ZnO solution (PDD + ZnO).

respect to the carbonate and phenyl peaks, as in UD samples (Fig. 1). Similarly, the intensity of peaks at 1,246/1,270 (amide III), 1,450 (CH), and 1,667 (amide I) cm^{-1} were recovered (Figs. 1, 4) after the partial demineralization process (Fig. 2). This indicates that the molecular structure of collagen is not noticeably altered (Xu & Wang, 2011) and that further stabilization of intra and intermolecular cross-links is provided (Daood et al., 2013) as an increase in the amine reaction sites provided the formation of ionic complexes with the collagen molecule. This provides substantial stability of the collagen fibrillar network (Daood et al., 2013). The amide III-band results from the NH in-plane deformation coupled to CN-stretching, whereas the amide-I band is associated with the stretching-vibration of the peptide carbonyl group (Fawzy et al., 2012). On the other hand, the protein-dependent spectral signal at 1,003 cm^{-1} (phenylalanine) decreased after immersing the PDD samples in CHX, preceding the appearance of the phosphate stretching peak at 960 cm^{-1}. This indicates that nucleation is a multi-step process involving both protein and mineral transition (Wang & Yao, 2010) and suggests a temporally synchronized process (Wang & Yao, 2010).

Raman spectral analysis showed an increase in the apparent relative mineral concentration, revealing the presence of new phosphate (960 cm^{-1}) and carbonate (1,070 cm^{-1}) (Fig. 4) precipitation which partially disappeared after 15 s of dentin demineralization as observed within the band of HA, the most intense peak of the spectrum (Fig. 2). These mineral aggregates contributed to development of crystallinity (Fig. 4), yielding spheroid crystals of β-type carbonated HA that is typical of crystals grown in the presence of high carbonate concentrations. However, the process does not lead to the direct crystallization of apatite, but to the nucleation of ACP $[Ca_x(PO_4)_y]$ (Seah et al., 2009). The ACP precursors (Dey et al., 2010) octocalcium phosphate $[Ca_8H_2(PO_4)_6 \cdot 5H_2O]$ and tricalcium phosphate $[Ca_3(PO_4)_2]$ phases have also been identified as precursors (Lussi & Linde, 1993).

The thermodynamic performance of this process and the specificity of the nucleation are conditioned, in summary, by the presence of interfaces of all sorts, from hydrophobic surface layers to organic macromolecules and in the structure of hydration layers around inorganic cations and anions (Veis & Dorvee, 2013). Nevertheless, it must be borne in mind that some remineralization processes may occur mainly by growth of residual crystals in the PDD tissue (Lussi & Linde, 1993). Additionally, CHX digluconate has been identified as a zinc chelator (Mohammadi & Abbott, 2009; Tallant et al., 2010) present in the current solution as a component of AS, which could contribute to

new mineral formation (Toledano et al., 2012*b*). Whether this procedure is by simple mineral precipitation between the collagen fibril (extrafibrillar) or by functional remineralization (intrafibrillar) should be ascertained.

The prenucleation clusters form loosely packed negatively charged highly mobile diffuse structures. Positively charged regions exist in a collagen fibril at the border of the gap and overlap zones. The nanosized, positively charged region can be used for mineral infiltration as well as charge–charge attraction (Cölfen, 2010; Nudelman et al., 2010), resulting in higher energy (Daood et al., 2013). In this way, the binding between some acidic noncollagenous proteins (dentin matrix protein 1) and collagen are also driven by electrostatic interactions. Variations produced in the mineral content from PDD to TDD substrates might have changed both the surface-free energy and the ζ potential of dentin (Erickson, 1992) throughout the mineralization process. Substrates (PDD and TDD) were characterized as scarcely wettable, after demineralization. Once immersed in CHX for 30 min, wettability significantly increased in both etching procedures (Table 1) confirming the optimal incorporation or deposition of mineral into/on the collagen fibrils, which made the apparent relative mineral concentration increase (Fig. 4).

When PDD was immersed in AS, CA values were similar to those of the control. Clinically, saliva is readily available to potentially remineralize. Calcium and phosphate of simulated saliva solutions can also influence dentin remineralization (Hara et al., 2008). In the present study, no phosphate-based component was included in the AS solution. The composition of this solution was previously reported in MMPs-mediated collagen degradation studies (Osorio et al., 2011*a*, 2011*b*). This lack of phosphate in our study might have resulted in the absence of significance in CA measurements performed on PDD samples, although the role of phosphate ions in aiding nucleation of apatite on a biological surface has been reported (Nicholson, 2002). Additionally, Kawasaki et al. (1999) reported that the immobilized phosphoproteins are thought to supply phosphate for mineralization, being capable of modulating crystal nucleation and growth, as well as binding to the collagenous network (Baht et al., 2010). This residual phosphate (960 cm^{-1}) could be detected in Raman analysis (Fig. 2) with a lower relative intensity than observed in UD samples (Fig. 1). On the contrary, wettability significantly decreased when TDD samples were immersed in AS. Remineralization of dentin substrate may depend upon the quality and quantity of the mineral and/or organic component remaining in the structure (Clarkson et al., 1991). Raman analysis (Fig. 5) showed both high crystallinity (narrow peak of the phosphate band) and high apparent gradient of mineral content (remarkable height of carbonate and phosphate peaks related to the HA band).

Observing the Raman spectra of the N–H and C–N peaks included in the 1,220–1,300 shift (Fig. 5), in junction with PS (Fig. 6), $ZnCl_2$ (Fig. 7), and ZnO (Fig. 8) reflected a change with respect to the position shown in UD (Fig. 1), PDD (Fig. 2), TDD (Fig. 3), and CHX (Fig. 4). This variation deserves further research.

Immersion of PDD samples in AS resulted in a significant negative increase of ζ potential (-1.16). Immersing TDD samples in AS resulted in a more negative value (-6.22) (Table 2). Acidic noncollagenous proteins, as polyanionic protein molecules, possess high calcium binding capacity (Wallwork et al., 2002; Gu et al., 2010). The phosphorylated collagen results in a highly negatively charged surface, reproducing the assessed negative ζ potential (Table 2) and acting as a virtual sink for the binding of calcium (Linde et al., 1989; Gu et al., 2010). Calcium ions present in the systems probably interact in the adsorption process and furthermore act as ligands between negatively charged groups. The adsorption of negatively charged molecules to dentin is based on ion-exchange processes, and calcium ions play an important role (Young et al., 1997). Electrostatic forces make possible the subsequent absorption of calcium ions onto the surface of the phosphorylated collagen, which eventually precipitate to form calcium phosphate clusters and grow into apatite nuclei (Gu et al., 2010). Figure 5 shows a well-defined peak of phosphate, demonstrating the precipitation of these ions in a matrix where the organic content, represented by phenylalanine and hydroxyproline, are proportionally more augmented (Fig. 5). Hydroxyproline imparts stability and rigidity to the triple-helix coil within the collagen molecule (Daood et al., 2013). TDD represents the ideal substrate to test the remineralizing ability of the demineralized collagen. Charge interactions become more pronounced when hydrophobicity decreases (Young et al., 1997), as CA significantly decreased after immersing the TDD specimens in the different remineralization solutions. In our study, the pH ranged from 6 to 6.24. It is well known that, apart from the pH, both calcium and phosphate ions play a major role in determining the ζ potential. Calcium ions make the ζ potential more positive and phosphate ions make it more negative (Young et al., 1997).

PDD specimens immersed in PS, showed the highest values of wettability (Table 1) and positive ζ potential (Table 2). CAs increased and ζ potential decreased, both significantly, when dentin was completely demineralized (TDD). The presence, the degree of saturation, and concentration of phosphate are relevant factors that influence dentin remineralization (Hara et al., 2008). Mineral induction by dentin collagen requires a minimum concentration of phosphate ester on the collagen. Saito et al. (1998) indicated that this value is greater than 2 mols per P/mol of collagen. At this level of phosphorylation, 19 mol of Ca/mol of collagen was found in the mineralizing medium. Around physiological pH and ionic strength (Veis & Dorvee, 2013) phosphate ions interact avidly with calcium ions. But, according to the classical nucleation theory, at some critical concentration of these ions their favorable interactions stabilize the ion cluster (Veis & Dorvee, 2013). This increases the electrostatic equilibrium or ζ potential (Table 2), which complies with the thermodynamic performance of the crystalline phase on the PDD surface. This is controlled by the magnitude of

the energy barrier of cluster formation, thus including the free energy of formation of a new surface (Veis & Dorvee, 2013). The ζ potential values were modulated by the degree of dentin demineralization and the electrostatic interaction attraction of the oppositely charged ions (mainly, calcium and phosphate), and by the restrictions on the mobility of the bound first-layer of water, which is different than the stable layers of water (Veis & Dorvee, 2013).

Nucleation represents an activation energy barrier to the formation of a solid phase from a supersaturated metastable solution. In biological environments, the activation energy for nucleation can be reduced by lowering of the interfacial energy (Ito et al., 2012), which reproduces the CA (Wege et al., 2003). The higher CA observed in TDD samples may be explained by the lower content of remaining ions characteristic of this substrate, after 12 h of demineralizing process, as the more stable crystalline phase becomes more favorable as more particles are added to the aggregate (Veis & Dorvee, 2013) as in PDD samples. This scarce content of remaining ions can be observed in Figure 3. High levels of phosphate at physiological pH favored the nucleation of HA precursors with lower calcium phosphate (Hara et al., 2008), and even ACP (LeGeros et al., 1999), as observed in Figure 6. This indicates a higher amount of consumed precursors as the carbonate peak decreased. Our Raman spectra also show a lower intensity of pyridinium peak, probably indicating the presence of both a lower cross-linked collagen (Xu & Wang, 2011) and a greater solid phase, as corroborated by the high crystallinity pattern and the higher apparent relative mineral concentration that reflects the analysis. The amide I and amide III shifts for cross-linked dentin specimens were toward lower frequencies, denoting a declined cross-linking of collagen that results after nucleation. Additionally, the remineralizing potential was clearly measurable with 2 ppm sodium fluoride in the PS. This supports either the theory of growth of residual mineral, or that fluoride acts as a nucleating agent (Kawasaki et al., 1999; Ito et al., 2012). The increase in fluoride concentration changed the mineral saturation level favoring fluorapatite formation.

Immersion of demineralized dentin in both $ZnCl_2$ and ZnO promoted a decrease in the CA values which was larger in PDD samples. TDD resulted in the lowest wettable substrate (Table 1). ZnO is an amphoteric oxide that has basic properties. It is nearly insoluble in water and alcohol, but it is soluble and degraded in acidic conditions. When placed in dentin it preferentially demonstrates direct contact with the demineralized dentin (Toledano et al., 2012*b*). Higher solubility of ZnO when in contact with acid substrates, as in some acidic noncollagenous proteins (dentin matrix proteins), could also account for the effective release of zinc ions (Toledano et al., 2012*b*). $ZnCl_2$ is highly acidic, soluble, and hydrophilic. It rapidly diffuses throughout the substrate, thereby over-demineralizing the underlying dentin (Osorio et al., 2011*b*), probably producing an increase in local ions available for further mineral growth. Immersion of PDD specimens, not only in $ZnCl_2$ and ZnO, but in all solutions, confirmed this effect as mineral crystallinity increased. As shown by data plotted by the reduced full width and extended height at half maximum of the phosphate band at 960 cm^{-1} (Figs. 7, 8). The more narrow the peak, the more crystalline (Schwartz et al., 2012).

Zinc ions inhibit MMPs and reduce collagen degradation in demineralized dentin (Osorio et al., 2011*c*). Selectivity for a specific MMP may be a function of differences in Zn/Ca ratios (McCall et al., 2000; Tezvergil-Mutluay et al., 2010). Zinc promotes binding between collagen and other oligomeric matrix proteins. Protein–protein interactions are controlled by the presence of metallic cations and dictated by zinc ions as the preferential ligand (Heinz et al., 2009). Partial demineralization of a mineralized collagen matrix by acids exposes the collagen scaffold to be remineralized, but also activates the pro-forms of dentin MMPs. Effective inhibitors of MMPs may protect the seed crystallite-sparse collagen fibrils of the scaffold from degradation before they can be re-mineralized (Liu et al., 2011). Zinc has a structural role in proteins. In structural zinc sites, zinc ions mainly stabilize tertiary structure of the protein. Four defined zinc-binding sites have been found in collagen molecules at the same locations as the collagenase cleavage sites (Rosenberg et al., 1998). This stabilization was confirmed after studying the shift of the molecular conformation from PDD (Fig. 2) and after immersing this substrate into both Zn solutions (Figs. 7, 8), quite similar to the spectra of UD (Fig. 1). The appearance of a new peak in the amide III band, in junction with AS (Fig. 5) and PS (Fig. 6) needs further research. As a result, it seems that subtle conformational changes may occur following zinc binding leading to the protection of sensitive cleavage sites of metalloproteinases.

The high relative intensity of the peak corresponding to the pyridinium ring, which appeared sharper and accentuated, was associated with a nonreducible cross-linking formation demonstrating that the first remineralization is intra-fibrillar, due to the clear and well-defined spectra of crystallinity (Fig. 7). This confirms that collagen is an active scaffold for the formation of oriented crystalline HA inside the fibrils (Cölfen, 2010; Nudelman et al., 2010). Furthermore, hydroxyproline showed a noticeable band that corresponds with the protective effect of Zn derivatives on stability of the sub-fibrillar triple-helical structure of collagen (Carrilho et al., 2010; Fawzy et al., 2012), indicating tissue–collagen concentration (Lamparter et al., 2002). Nevertheless, the peak was relatively smooth indicating there was mineral precipitation on the collagen web. Binding models exist that predict the existence of a single binding site on a protein molecule and indicate preferential high affinity for a specific cationic species, whereas the existence of multiple binding sites can accommodate different cations with different affinities for the protein molecule (Heinz et al., 2009). Amino acid side chains serving as zinc ligands in these structures often create hydrogen bond contacts with other residues to three-dimensionally orient the binding site configuration and lower the entropy for binding of the metallic ion (McCall et al., 2000). Zinc-bound water is a hydrogen bond donor (McCall et al., 2000), and phosphoric acid-etched collagen

may act as a hydrogen bond acceptor. However, there is no predilection of a particular binding model based on current data; the data simply suggests that different divalent cations have different affinity constants to collagen.

On the other hand, PDD attained the highest ζ potential values among solutions, in junction with PS, when Zn compounds were used. TDD, when immersed in ZnO solution, showed an almost neutral value (0.06 mV) and $ZnCl_2$ resulted in a negative value ($\times$0.32 mV). Local variations in the mass ratio between Ca^{2+} and Zn^{2+} can alter the differential hydration free-energy of Zn^{2+}, as the latter is dependent on its co-ordination geometry of zinc–water. We speculate that zinc–water/protein interactions may have decreased the hydration free-energy of Zn^{2+} relative to the free energies of other divalent cations such as calcium (Sakharov & Lim, 2005). This differential metallic ion-binding affinity hypothesis is also indirectly supported by data available from other proteins such as metallothioneins (Nations et al., 2008).

Present results may explain, in part, the high clinical interest of engineering intervention in this early time point of dentin remineralization. Analysis of the limited literature available on dentin remineralization at 30 min of immersing demineralized collagen in remineralizing solutions indicates that further specific studies on the relationship between the dentin micro-nanostructure and the physicochemical properties of this treated substrate should be performed.

Acknowledgments

This work was supported by grants CICOM/FEDER MAT2011-24551, MAT2011-023339, and JA-P08-CTS-3944.

References

Baht, G.S., O'Young, J., Borovina, A., Chen, H., Tye, C.E., Karttunen, M., Lajoie, G.A., Hunter, G.K. & Goldberg, H.A. (2010). Phosphorylation of Ser 136 is critical for potent bone sialoprotein-mediated nucleation of hydroxyapatite crystals. *Biochem J* **428**, 385–395.

Bertassoni, L.E., Habelitz, S., Pugach, M., Soares, P.C., Marshall, S.J. & Marshall, G.W., Jr. (2010). Evaluation of surface structural and mechanical changes following remineralization of dentin. *Scanning* **32**, 312–319.

Bertassoni, L.E., Habelitz, S., Marshall, S.J. & Marshall, G.W. (2011). Mechanical recovery of dentin following remineralization *in vitro*—An indentation study. *J Biomech* **44**, 176–181.

Carrilho, M.R., Carvalho, R.M., Sousa, E.N., Nicolau, J., Breschi, L., Mazzoni, A., Tjäderhane, L., Tay, F.R., Agee, K. & Pashley, D.H. (2010). Substantivity of chlorhexidine to human dentin. *Dent Mater* **26**, 779–785.

Chun, M.S., Lee, S.Y. & Yang, S.M. (2003). Estimation of zeta potential by electrokinetic analysis of ionic fluid flows through a divergent microchannel. *J Colloid Interf Sci* **266**, 120–126.

Clarkson, B.H., Feagin, F.F., McCurdy, S.P., Sheetz, J.H. & Speirs, R. (1991). Effects of phosphoprotein moieties on the remineralization of human root caries. *Caries Res* **25**, 166–173.

Cölfen, H. (2010). Biomineralization: A crystal-clear view. *Nat Mater* **9**, 960–961.

Daood, U., Iqbal, K., Nitisusanta, L.I. & Fawzy, A.S. (2013). Effect of chitosan/riboflavin modification on resin/dentin interface: Spectroscopic and microscopic investigations. *J Biomed Mater Res A* **101**, 1846–1856.

Dey, A., Bomans, P.H., Müller, F.A., Will, J., Frederik, P.M., de With, G. & Sommerdijk, N.A. (2010). The role of prenucleation clusters in surface-induced calcium phosphate crystallization. *Nat Mater* **9**, 1010–1014.

Erickson, R.L. (1992). Surface interactions of dentin adhesive materials. *Oper Dent* **5**, 81–94.

Fawzy, A., Nitisusanta, L., Iqbal, K., Daood, U., Beng, L.T. & Neo, J. (2012). Characterization of riboflavin-modified dentin collagen matrix. *J Dent Res* **91**, 1049–1054.

Gu, L.S., Kim, J., Kim, Y.K., Liu, Y., Dickens, S.H., Pashley, D.H., Ling, J.Q. & Tay, F.R. (2010). A chemical phosphorylation-inspired design for type I collagen biomimetic remineralization. *Dent Mater* **26**, 1077–1089.

Hao, J., Ramachandran, A. & George, A. (2009). Temporal and spatial localization of the dentin matrix proteins during dentin biomineralization. *J Histochem Cytochem* **57**, 227–237.

Hara, A.T., Karlinsey, R.L. & Zero, D.T. (2008). Dentine remineralization by simulated saliva formulations with different Ca and Pi contents. *Caries Res* **42**, 51–56.

He, G. & George, A. (2004). Dentin matrix protein 1 immobilized on type I collagen fibrils facilitates apatite deposition *in vitro*. *J Biol Chem* **279**, 11649–11656.

Heinz, U., Hemmingsen, L., Kiefer, M. & Adolph, H.W. (2009). Structural adaptability of zinc binding sites: Different structures in partially, fully, and heavy-metal loaded states. *Chemistry* **27**, 7350–7358. [Published erratum in *Chemistry* 2009;**15**, 8664.]

Ito, S., Iijima, M., Motai, F., Mizoguchi, I. & Saito, T. (2012). Effects of calcium salts of acidic monomers on mineral induction of phosphoprotein immobilized to agarose beads. *J Biomed Mater Res A* **100**, 2760–2765.

Kawasaki, K., Ruben, J., Stokroos, I., Takagi, O. & Arends, J. (1999). The remineralization of EDTA-treated human dentine. *Caries Res* **4**, 275–280.

Kim, D.S., Kim, J., Choi, K.K. & Kim, S.Y. (2011). The influence of chlorhexidine on the remineralization of demineralized dentine. *J Dent* **39**, 855–862.

Kim, J., Uchiyama, T., Carrilho, M., Agee, K.A., Mazzoni, A., Breschi, L., Carvalho, R.M., Tjäderhane, L., Looney, S., Wimmer, C., Tezvergil-Mutluay, A., Tay, F.R. & Pashley, D.H. (2010). Chlorhexidine binding to mineralized versus demineralized dentin powder. *Dent Mater* **26**, 771–778.

Lamparter, S., Slight, S.H. & Weber, K.T. (2002). Doxycycline and tissue repair in rats. *J Lab Clin Med* **139**, 295–302.

LeGeros, R.Z., Bleiwas, C.B., Retino, M. & LeGeros, J.P. (1999). Zinc effect on the *in vitro* formation of calcium phosphates: Relevance to clinical inhibition of calculus formation. *Am J Dent* **12**, 65–70.

Li, Y., Thula, T.T., Jee, S., Perkins, S.L., Aparicio, C., Douglas, E.P. & Gower, L.B. (2012). Biomimetic mineralization of woven bone-like nanocomposites: Role of collagen cross-links. *Biomacromolecules* **13**, 49–59.

Linde, A., Lussi, A. & Crenshaw, M.A. (1989). Mineral induction by immobilized polyanionic proteins. *Calcif Tissue Int* **44**, 286–295.

Liu, Y., Mai, S., Li, N., Yiu, C.K., Mao, J., Pashley, D.H. & Tay, F.R. (2011). Differences between top–down and bottom–up approaches in mineralizing thick, partially demineralized collagen scaffolds. *Acta Biomaterialia* **7**, 1742–1751.

Lussi, A. & Linde, A. (1993). Mineral induction *in vivo* by dentine proteins. *Caries Res* **27**, 241–248.

Marshall, G.W., Jr., Inai, N., Wu-Magidi, I.C., Balooch, M., Kinney, J.H., Tagami, J. & Marshall, S.J. (1997). Dentin demineralization: Effects of dentin depth, pH and different acids. *Dent Mater* **13**, 338–343.

McCall, K.A., Huang, C. & Fierke, C.A. (2000). Function and mechanism of zinc metalloenzymes. *J Nutr* **130**, 1437S–1446S.

Mohammadi, Z. & Abbott, P.V. (2009). The properties and applications of chlorhexidine in endodontics. *Int Endod J* **42**, 288–302.

Montes Ruiz-Cabello, F.J., Rodríguez-Valverde, M.A., Marmur, A. & Cabrerizo-Vílchez, M.A. (2011). Comparison of sessile drop and captive bubble methods on rough homogeneous surfaces: A numerical study. *Langmuir* **27**, 9638–9643.

Nations, S.P., Boyer, P.J., Love, L.A., Burritt, M.F., Butz, J.A., Wolfe, G.I., Hynan, L.S., Reisch, J. & Trivedi, J.R. (2008). Denture cream: An unusual source of excess zinc, leading to hypocupremia and neurologic disease. *Neurology* **71**, 639–643.

Nicholson, R. (2002). *The Chemistry of Medical and Dental Materials*, p. 92. Cambridge, UK: Royal Society of Chemistry.

Nudelman, F., Pieterse, K., George, A., Bomans, P.H., Friedrich, H., Brylka, L.J., Hilbers, P.A., de With, G. & Sommerdijk, N.A. (2010). The role of collagen in bone apatite formation in the presence of hydroxyapatite nucleation inhibitors. *Nat Mater* **9**, 1004–1009.

Osorio, R., Yamauti, M., Osorio, E., Román, J.S. & Toledano, M. (2011*a*). Zinc-doped dentin adhesive for collagen protection at the hybrid layer. *Eur J Oral Sci* **119**, 401–410.

Osorio, R., Yamauti, M., Osorio, E., Ruiz-Requena, M.E., Pashley, D., Tay, F. & Toledano, M. (2011*b*). Effect of dentin etching and chlorhexidine application on metalloproteinase-mediated collagen degradation. *Eur J Oral Sci* **119**, 79–85.

Osorio, R., Yamauti, M., Osorio, E., Ruiz-Requena, M.E., Pashley, D.H., Tay, F.R. & Toledano, M. (2011*c*). Zinc reduces collagen degradation in demineralized human dentin explants. *J Dent* **39**, 148–153.

Panighi, M. & G'Sell, C. (1992). Influence of calcium concentration on the dentin wettability by an adhesive. *J Biomed Mater Res* **26**, 1081–1089.

Pascon, F.M., Kantovitz, K.R., Soares, L.E., Santo, A.M., Martin, A.A. & Puppin-Rontani, R.M. (2012). Morphological and chemical changes in dentin after using endodontic agents: Fourier transform Raman spectroscopy, energy-dispersive X-ray fluorescence spectrometry, and scanning electron microscopy study. *J Biomed Opt* **17**, 075008.

Rosenberg, K., Olsson, H., Mörgelin, M. & Heinegård, D. (1998). Cartilage oligomeric matrix protein shows high affinity zinc-dependent interaction with triple helical collagen. *J Biol Chem* **273**, 20397–20403.

Sadat-Shojai, M., Atai, M., Nodehi, A. & Khanlar, L.N. (2010). Hydroxyapatite nanorods as novel fillers for improving the properties of dental adhesives: Synthesis and application. *Dent Mater* **26**, 471–482.

Saito, T., Yamauchi, M. & Crenshaw, M.A. (1998). Apatite induction by insoluble dentin collagen. *J Bone Miner Res* **13**, 265–270.

Sakharov, D.V. & Lim, C. (2005). Zn protein simulations including charge transfer and local polarization effects. *J Am Chem Soc* **127**, 4921–4929.

Schwartz, A.G., Pasteris, J.D., Genin, G.M., Daulton, T.L. & Thomopoulos, S. (2012). Mineral distributions at the developing tendon enthesis. *PLoS One* **7**, e48630.

Seah, R.K.H., Garland, M., Loo, J.S.C. & Widjaja, E. (2009). Use of Raman microscopy and multivariate data analysis to observe the biomimetic growth of carbonated hydroxyapatite on bioactive glass**.** *Anal Chem* **81**, 1442–1449.

Silver, F.H. & Landis, W.J. (2011). Deposition of apatite in mineralizing vertebrate extracellular matrices: A model of possible nucleation sites on type I collagen. *Connect Tissue Res* **52**, 242–254.

Tallant, C., Marrero, A. & Gomis-Rüth, F.X. (2010). Matrix metalloproteinases: Fold and function of their catalytic domains. *Biochim Biophys Acta* **1803**, 20–28.

Tezvergil-Mutluay, A., Agee, K., Hoshikac, T., Carrilho, M., Breschi, L., Tjäderhane, L., Nishitani, Y., Carvalho, R.M., Looney, S., Tay, F.R. & Pashley, D.H. (2010). The requirement of zinc and calcium ions for functional MMP activity in demineralized dentin matrices. *Dent Mater* **26**, 1059–1067.

Toledano, M., Osorio, E., Aguilera, F.S, Cabrerizo-Vilchez, M.A. & Osorio, R. (2012*a*). Surface analysis of conditioned dentin and resin-dentin bond strength. *J Adhes Sci Technol* **26**, 27–40.

Toledano, M., Osorio, R., de Leonardi, G., Rosales-Leal, J.I., Ceballos, L. & Cabrerizo-Vílchez, M.A. (2001). Influence of self-etching primer on the resin adhesion to enamel and dentin. *Am J Dent* **14**, 205–210.

Toledano, M., Sauro, S., Cabello, I., Watson, T. & Osorio, R. (2013). A Zn-doped etch-and-rinse adhesive may improve the mechanical properties and the integrity at the bonded-dentine interface. *Dent Mater* **29**, 142–152.

Toledano, M., Yamauti, M., Ruiz-Requena, M.E. & Osorio, R. (2012*b*). A ZnO-doped adhesive reduced collagen degradation favouring dentine remineralization. *J Dent* **40**, 756–765.

Veis, A. & Dorvee, J.R. (2013). Biomineralization mechanisms: A new paradigm for crystal nucleation in organic matrices. *Calcif Tissue Int* **93**, 307–315.

Wallwork, M.L., Kirkham, J., Chen, H., Chang, S.X., Robinson, C., Smith, D.A. & Clarkson, B.H. (2002). Binding of dentin noncollagenous matrix proteins to biological mineral crystals: An atomic force microscopy study. *Calcif Tissue Int* **71**, 249–255.

Wang, Y. & Yao, X. (2010). Morphological/chemical imaging of demineralized dentin layer in its natural, wet state. *Dent Mater* **26**, 433–442.

Wege, H.A., Aguilar, J.A., Rodriguez-Valverde, M.A., Toledano, M., Osorio, R. & Cabrerizo-Vilchez, M.A. (2003). Dynamic contact angle and spreading rate measurements for the characterization of the effect of dentin surface treatments. *J Colloid Interf Sci* **263**, 162–169.

Xu, C. & Wang, Y. (2011). Cross-linked demineralized dentin maintains its mechanical stability when challenged by bacterial collagenase. *J Biomed Mater Res B Appl Biomater* **96**, 242–248.

Xu, Z., Neoh, K.G., Lin, C.C. & Kishen, A. (2011). Biomimetic deposition of calcium phosphate minerals on the surface of partially demineralized dentine modified with phosphorylated chitosan. *J Biomed Mater Res B Appl Biomater* **98**, 150–159.

Young, A., Smistad, G., Karlsen, J., Rölla, G. & Rykke, M. (1997). Zeta potentials of human enamel and hydroxyapatite as measured by the Coulter DELSA 440. *Adv Dent Res* **11**, 560–565.

Zerella, J.A., Fouad, A.F. & Spångberg, L.S. (2005). Effectiveness of a calcium hydroxide and chlorhexidine digluconate mixture as disinfectant during retreatment of failed endodontic cases. *Oral Surg Oral Med Oral Pathol Oral Radiol Endod* **100**, 756–761.